Crystal orientation dependence of interfacial magnetic anisotropy at heavy-metal/magnetic-garnet interfaces

Aidan J. Lee,* Side Guo,* Adam S. Ahmed, and Fengyuan Yang
Department of Physics, The Ohio State University, Columbus, Ohio 43210, USA

(Received 12 August 2020; accepted 9 November 2020; published 23 November 2020)

Ferrimagnetic insulators capped with a heavy metal are becoming an increasingly interesting materials system in spintronics due to their unique ability for electrical manipulation and detection of magnetic states and spin textures via spin-orbit torques. The ability to engineer magnetic anisotropy is a powerful tool for tuning the recently discovered phenomena in these bilayers such as electrical switching or the stabilization of topological magnetic textures. We observe large shifts in the magnetic anisotropy in $Tm_3Fe_5O_{12}$ and $Y_3Fe_5O_{12}$ thin films due to heavy-metal capping layers, which strongly depends on the orientation of the substrate and therefore the orientation of the epitaxial films. This work suggests large Rashba spin-orbit coupling at the metal/ferrimagnetic-insulator interface, which can be engineered in spintronic devices that utilize spin-orbit torques for electrical control of the magnetization in magnetic insulators.

DOI: 10.1103/PhysRevB.102.174434

I. INTRODUCTION

Advances in epitaxial growth of high-quality magnetic insulator films approaching single nanometer thickness have enabled the emergence of novel interface-driven phenomena in heavy-metal/magnetic-insulator systems, such as topological spin textures and electrical controllability. These phenomena take advantage of the spin Hall effect in an adjacent heavy-metal layer that generates a large spin-orbit torque (SOT) which can be used to detect and manipulate the magnetization of the insulating layer [1]. Critical to these new discoveries is the magnetic anisotropy, which is a powerful tool for navigating the phase space for stabilizing magnetic skyrmions as well as determining the SOT that is necessary to alter the magnetization [2,3]. As the magnetic insulator becomes extremely thin, interfacial interactions that generate additional anisotropy can dictate the overall magnetic landscape. Interfacial interactions have been widely studied in metallic multilayers, such as interface-induced perpendicular magnetic anisotropy [4,5] as well as magnetic skyrmions induced by the interfacial Dzyaloshinskii-Moriya interaction [6–9]. However, very little work has focused on understanding the interfacial interactions in heterostructures with insulating magnetic layers, which have advantageous properties such as high frequency dynamics and low magnetic damping as well as a lack of resistive heating in the magnetic insulator layers. Recent reports of topological Hall effect [10–13], efficient electrical switching [1,3], and fast domain wall propagation [14,15] in heavy-metal/ferrimagnetic insulator (FMI) based interfacial systems that take advantage of a large SOT have made magnetic insulators a promising materials platform for integration into spintronic devices. Therefore, fundamental interfacial interactions in these heterostructures need to be further investigated.

Recent reports have demonstrated that symmetry breaking at the interface between a nonmagnetic material (NM) and a FMI induces interfacial Rashba spin-orbit coupling (SOC), leading to an interfacial magnetic anisotropy which dominates the magnetism in very thin FMI films [16,17]. In this paper, we report a systematic dependence of interfacial magnetic anisotropy on the crystal orientation of epitaxial $Tm_3Fe_5O_{12}$ (TmIG) and $Y_3Fe_5O_{12}$ (YIG) thin films capped with Pt and Au. The obtained interfacial anisotropy is up to 3255 G, which is very large compared with the magnetocrystalline and shape anisotropy of the garnet films [16], and varies by a factor of 5 depending on the orientation of the garnet films and choice of metallic capping layer. The strong dependence of interfacial anisotropy on the crystal orientation of the FMI suggests that the symmetry of the crystal lattice at the interface plays a critical role in the interfacial magnetic anisotropy.

II. EXPERIMENTAL DETAILS

We grow epitaxial TmIG and YIG films on (100)-, (110)-, and (111)-oriented $Gd_3Ga_5O_{12}$ (GGG) substrates by off-axis sputtering [11,18,19]. The high quality of TmIG(111) and YIG(111) films has been confirmed in our previous reports using x-ray diffraction (XRD), scanning transmission electron microscopy, and atomic force microscopy (AFM) [11,17]. Figure 1 shows the 2θ-ω XRD scans of 35-nm TmIG and YIG films grown on three orientations of GGG substrates, where the (100)- and (111)-oriented films exhibit pronounced Laue oscillations that stem from the interference of two kinds of x-ray diffractions: one by the conventional crystalline atomic planes and the other by the whole film thickness between the top surface and the interface with the substrate. Thus, Laue oscillations only arise in highly uniform, single-crystalline ordered films. The lack of Laue oscillations in the (110)-oriented film is not fully understood at this time, which may be due to two possible reasons: (1) the surface quality of the GGG(110) substrate is not as good as the (111) and (100)

*These authors contributed equally to this work.

 ©2020 American Physical Society

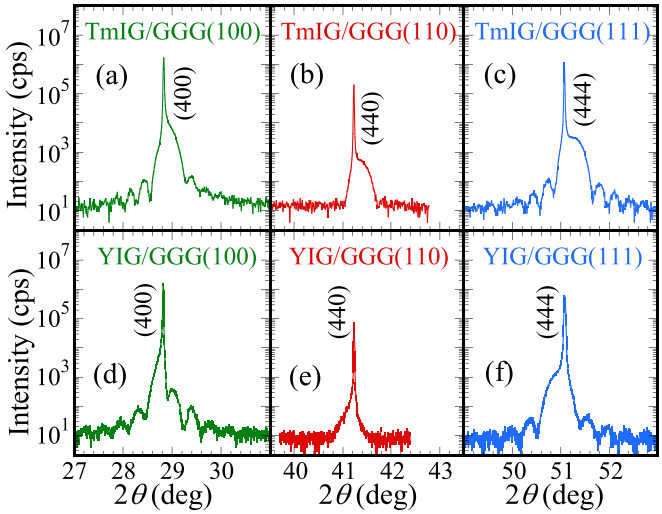

FIG. 1. Characterization of crystalline quality by x-ray diffraction. 2θ-ω XRD scans of 35 nm (a)–(c) TmIG and (d)–(f) YIG films grown on (100)-, (110)-, and (111)-oriented GGG.

substrates, and (2) the (110) plane is the least-preferred orientation for epitaxial growth of the garnet films. The TmIG and YIG films exhibit very narrow XRD rocking curves, indicating high crystalline quality [11,20]. Our previous x-ray reflectivity measurements also demonstrate sharp Pt/YIG and Au/YIG interfaces [20,21]. Figure 2 shows the AFM scans over a 5-μm × 5-μm region of the garnet films of all three orientations. All six films have smooth surfaces with a root-mean-square roughness ranging from 0.12 to 0.21 nm. A smooth surface of these films and the sharp interfaces with metals are critical for the investigation of strong interfacial magnetic anisotropy in these structures.

III. RESULTS AND DISCUSSION

In order to determine the interfacial anisotropy in NM/FMI bilayers, we first measure the magnetic anisotropy in the bare TmIG (5 nm) and YIG (5 nm) films using angular dependent ferromagnetic resonance (FMR) in a cavity with a microwave frequency, $f = 9.66$ GHz. Figures 3(a) and 3(c) show representative FMR derivative spectra for the TmIG(111) and YIG(100) films (two of the six films: two FMIs and three orientations), respectively, at various polar angles θ_H between the applied magnetic field (H) and the film normal. As the sample is rotated from in-plane (IP) ($\theta_H = 90°$) to out-of-plane (OOP) ($\theta_H = 0°$), the resonance field H_{res} increases, which is determined by fitting the FMR spectra to a modified derivative of the Lorentzian function [22],

$$\frac{dI}{dH}(H_{res}, \Delta H) = a\,\frac{(H - H_{res})\left(\frac{\Delta H}{2}\right)^2}{\left[\left(\frac{\Delta H}{2}\right)^2 + (H - H_{res})^2\right]^2} + b\,\frac{\left(\frac{\Delta H}{2}\right)^3}{\left[\left(\frac{\Delta H}{2}\right)^2 + (H - H_{res})^2\right]^2}, \quad (1)$$

where a and b are fitting parameters and in the limit of $a \gg b$, $\Delta H = \sqrt{3}\Delta H_{pp}$ (ΔH_{pp} is the peak-to-peak linewidth). The angular dependence of H_{res} for bare TmIG and YIG is shown

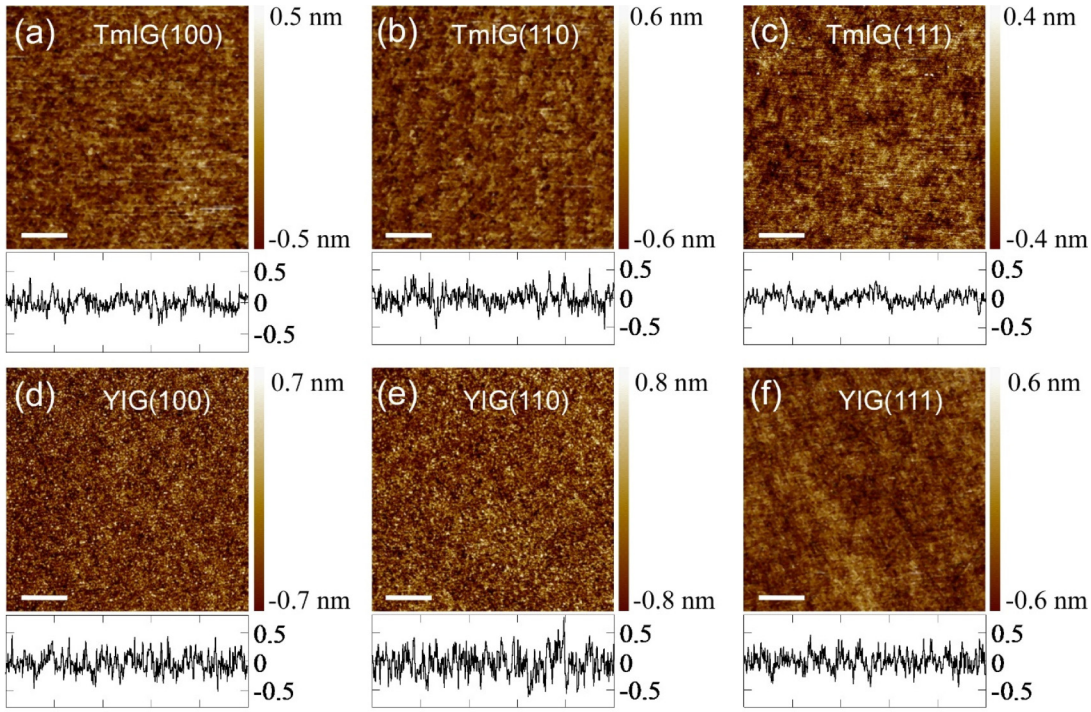

FIG. 2. Surface roughness by atomic force microscopy. AFM images of (a)–(c) TmIG and (d)–(f) YIG films grown on (100)-, (110)-, and (111)-oriented GGG substrates. The height profile (unit: nm) below each AFM image is a horizontal line cut at the middle of the AFM image. The root-mean-square surface roughness of the films are (a) TmIG(100): 0.16 nm; (b) TmIG(110): 0.17 nm; (c) TmIG(111): 0.12 nm; (d) YIG(100): 0.18 nm; (e) YIG(110): 0.21 nm; and (f) YIG(111) 0.16 nm. Scale bar: 1 μm.

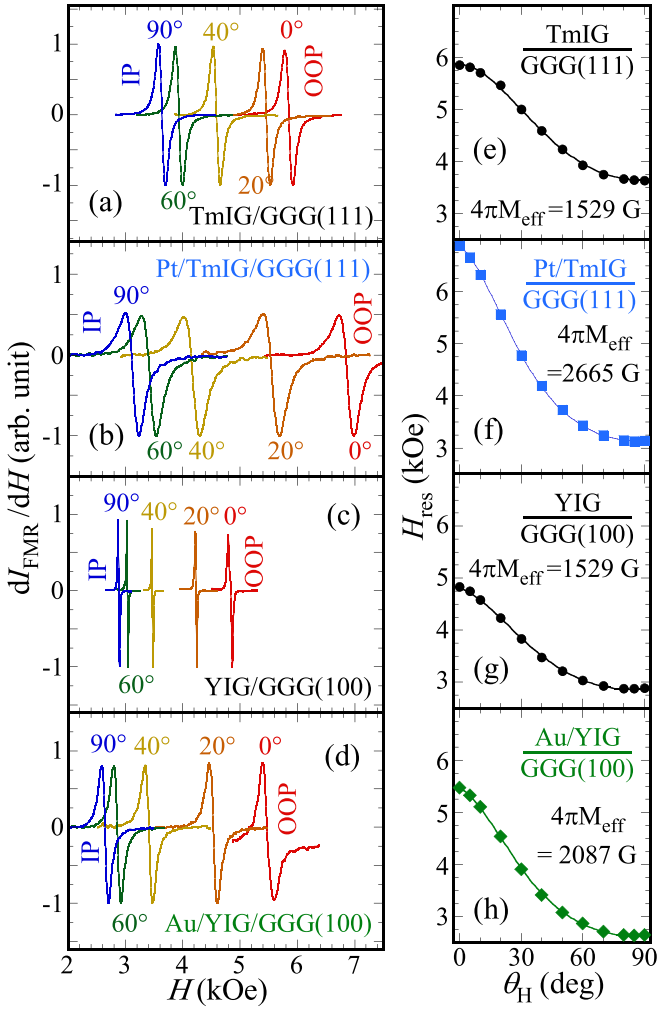

FIG. 3. Angular dependent ferromagnetic resonance. Representative FMR spectra of TmIG (5 nm)/GGG(111) films at various polar angles (a) before and (b) after the film was capped with Pt. The same is shown for YIG (5 nm)/GGG(100) (c) before and (d) after the film was capped with Au. (e)–(h) Resonance fields as a function of the polar angle θ_H extracted from their respective FMR spectra to their left, which are fit to obtain $4\pi M_{eff}$ of (e) TmIG(111): 1529 ± 20 G; (f) Pt/TmIG(111): 2665 ± 16 G; (g) YIG/GGG(100): 1529 ± 24 G; and (h) Au/YIG(100): 2087 ± 17 G.

in Figs. 3(e) and 3(g), which are fit to determine the effective saturation magnetization $4\pi M_{eff}$ and gyromagnetic ratio γ. The OOP uniaxial anisotropy $H_\perp$ can then be determined using $4\pi M_{eff} = 4\pi M_s - H_\perp$ where $4\pi M_s$ is the saturation magnetization. In order to fit H_{res} vs θ_H, the following fitting procedure is applied: First, the free energy density for a magnetic film is given by [23–26]

$$F = -\boldsymbol{H}\cdot\boldsymbol{M} + \tfrac{1}{2}M(4\pi M_{eff})\cos^2\theta, \qquad (2)$$

where θ is the OOP polar angle of the equilibrium magnetization, $\boldsymbol{M}$. Equation (2) is numerically minimized to determine the direction of $\boldsymbol{M}$. Higher order contributions for the free energy density are found to be negligible and ignored [17,23]. Equation (2) is then substituted into the FMR condition

$$\left(\frac{\omega}{\gamma}\right)^2 = \frac{1}{M^2\sin^2\theta}\left[\frac{\partial^2 F}{\partial\theta^2}\frac{\partial^2 F}{\partial\phi^2} - \left(\frac{\partial^2 F}{\partial\phi\partial\theta}\right)^2\right], \qquad (3)$$

where ω is the angular frequency of the applied microwaves and ϕ is the in-plane azimuthal angle of the magnetization. By combining Equations (1)–(3), H_{res} can be calculated at any given applied field direction, which is then fit to the experimental data to obtain $4\pi M_{eff}$. The fits to the resonance fields and the resulting $4\pi M_{eff}$ are shown in Figs. 3(e) and 3(g), which agree well with the experimental data. Coincidently, $4\pi M_{eff}$ is the same for the TmIG/GGG(111) and YIG/GGG(100) films; however, the values of $\gamma/2\pi$ are 22.3 and 27.7 GHz T^{-1}, respectively, which accounts for the difference in their angular dependence of H_{res}. Note that in both films the resonance field is maximized in the out-of-plane direction, minimized in the in-plane direction, and $4\pi M_{eff} > 0$, which indicate that these films all have an easy axis that lies in the plane of the film. Furthermore, previous studies have found that any uniaxial or cubic in-plane anisotropies are negligible in thin TmIG and YIG films and can therefore be described as having an easy-plane anisotropy [17,25].

After FMR characterization of the bare FMI films, the TmIG and YIG films are capped with 2-nm Pt or 8-nm Au at room temperature and then measured again using FMR to determine the new $4\pi M_{eff}$. The two NM capping layers were chosen for the following reasons: (1) our previous study found that both Pt and Au induce a substantial change to $4\pi M_{eff}$ [17]; (2) there is an abundance of studies that involve Pt or Au grown on TmIG or YIG for the purposes of studying spin pumping or the presence of an interfacial Dzyaloshinskii-Moriya interaction, yet essentially none of them discuss in detail the interfacial anisotropy of the NM/FMI bilayers; (3) both Pt and Au are highly stable in air. Figures 3(b) and 3(d) show representative FMR derivative spectra of Pt/TmIG(5 nm)/GGG(111) and Au/YIG(5 nm)/GGG(100), respectively (two of the 12 bilayers: two NMs, two FMIs, and three substrate orientations). Comparing the FMR spectra between Figs. 3(a) and 3(b) as well as between Figs. 3(c) and 3(d) demonstrates that the NM capping layer drastically alters the angular dependence of the resonance fields and broadens the spectra. The broadening of the linewidth after the addition of the Pt or Au overlayer is attributed to spin pumping from the FMI into the heavy metal, which has been shown to broaden the spectra and enhance the Gilbert damping [21]. The extracted $4\pi M_{eff}$ is shown in Figs. 3(f) and 3(h), which indicates a change of the effective saturation magnetization, $\Delta(4\pi M_{eff}) = 1136$ and 558 G for Pt on TmIG(111) and Au on YIG(100), respectively.

This same measurement is conducted on all 12 combinations of bilayers and the results are shown in Fig. 4. The angular dependencies of the resonance fields are overlaid before and after the FMI is capped with Pt or Au to clearly demonstrate the stark change in $4\pi M_{eff}$ and therefore anisotropy. For example, in Fig. 4(l) the bare YIG/GGG(110) has resonance fields ranging from 2686 Oe (in plane) to 5473 Oe (out of plane), while by capping it with Au its H_{res} shifts from 1011 to 8031 Oe. The value of $\Delta(4\pi M_{eff})$ is shown in each panel of Fig. 4. Depending on the orientation of the FMI

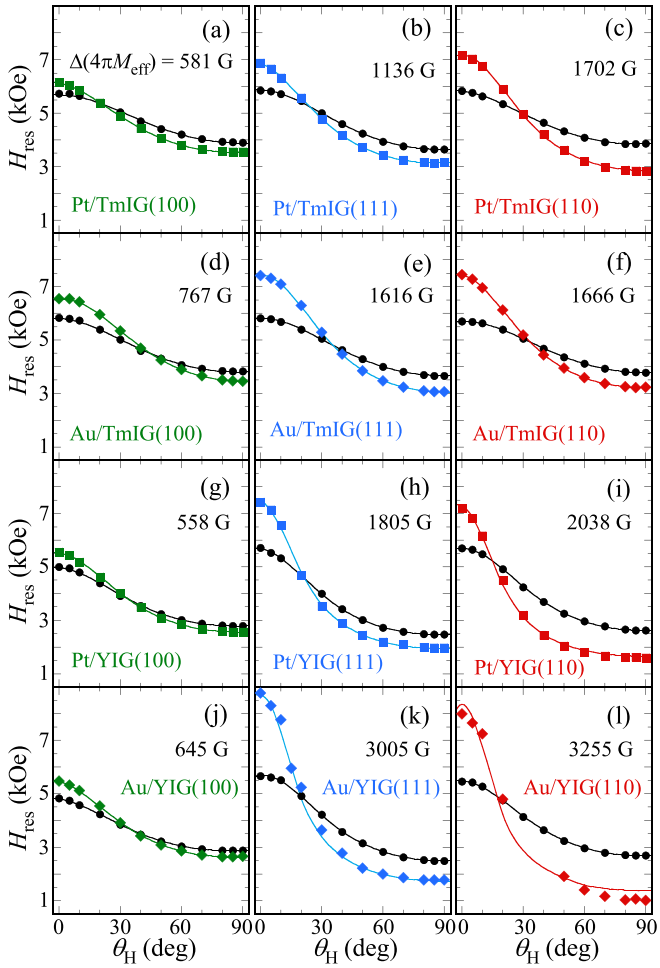

FIG. 4. Angular dependent ferromagnetic resonance of the garnet films before and after the deposition of the Pt or Au overlayer. Resonance fields as a function of the polar angle before (black circles) and after being capped with Pt (various colored squares) or Au (various colored diamonds) for three orientations of (a)–(f) TmIG (5 nm) films capped with (a)–(c) Pt or (d)–(f) Au as well as (g)–(l) YIG (5 nm) films capped with (g)–(i) Pt or (j)–(l) Au. The extracted $\Delta(4\pi M_{\rm eff})$ values are (a) Pt/TmIG(100): 581 ± 53 G; (b) Pt/TmIG(111): 1136 ± 36 G; (c) Pt/TmIG(110): 1702 ± 42 G; (d) Au/TmIG/(100): 767 ± 58 G; (e) Au/TmIG(111): 1616 ± 33 G; (f) Au/TmIG(110): 1666 ± 28 G; (g) Pt/YIG(100): 558 ± 50 G; (h) Pt/YIG(111): 1805 ± 73 G; (i) Pt/YIG(110): 2038 ± 89 G; (j) Au/YIG(100): 645 ± 41 G; (k) Au/YIG(111): 3005 ± 107 G; and (l) Au/YIG(110): 3255 ± 397 G.

and capping layer, $\Delta(4\pi M_{\rm eff})$ ranges from 558 ± 50 G for Pt/YIG/GGG(100) to 3255 ± 397 G for Au/YIG/GGG(110).

Note that the saturation magnetizations of TmIG and YIG, $4\pi M_{\rm s} = 1080$ and 1670 G, respectively, do not change after the deposition of Pt or Au, which results in $\Delta(4\pi M_{\rm eff}) = -\Delta H_{\perp}$. Since the magnetocrystalline anisotropy remains unchanged with the capping layer, the measured $-\Delta H_{\perp}$ solely arises from the interfacial magnetic anisotropy at the NM/FMI interface. The extracted values of $\Delta(4\pi M_{\rm eff})$ for all 12 combinations of bilayers are shown in Fig. 5, which illustrates a noteworthy and general trend. In all four combinations of NM/FMI bilayers, Pt/TmIG, Au/TmIG, Pt/YIG,

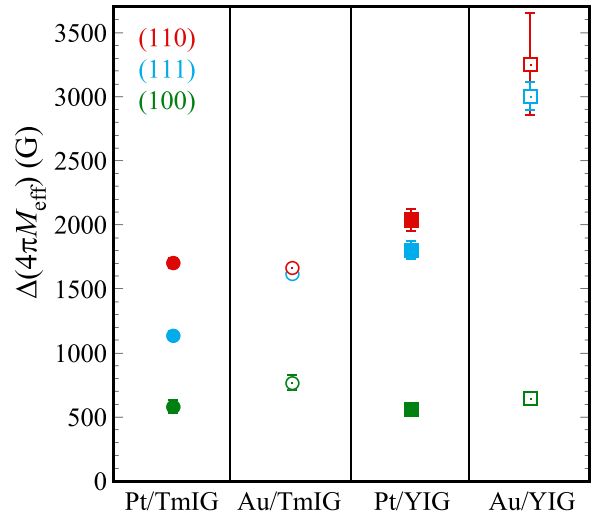

FIG. 5. Change in effective saturation magnetization. $\Delta(4\pi M_{\rm eff})$ for (110) (red), (111) (blue), and (100) (green) oriented TmIG and YIG films capped with either Pt or Au. In all cases $\Delta(4\pi M_{\rm eff})$ is largest for (110)-oriented FMIs and smallest for (100)-oriented FMIs.

and Au/YIG, the (110)-oriented FMIs exhibit the largest $\Delta(4\pi M_{\rm eff})$, followed by the (111)-oriented FMIs, and finally the (100)-oriented FMIs with the smallest $\Delta(4\pi M_{\rm eff})$.

The six AFM images in Fig. 2 demonstrate comparably smooth surfaces of TmIG and YIG films in all three crystallographic orientations with a roughness of 0.12–0.21 nm. In addition, our previous x-ray reflectivity measurement and analysis showed an interfacial roughness of 0.1 and 0.2 nm in Au/YIG and Pt/YIG bilayers, respectively [20,21]. Thus, we can rule out that interfacial roughness is responsible for the systematic behavior in $\Delta(4\pi M_{\rm eff})$ for the four combinations of NM/FMI bilayers in three orientations. The trend in $\Delta(4\pi M_{\rm eff})$, and thus the interfacial magnetic anisotropy, with respect to the orientation of the FMI films appears to arise from the surface crystal structure of various orientations and the resulting effects that it has on the NM/FMI interfacial interactions. The same trend occurs in two different magnetic insulators and with two NMs, which gives some indication that the dependence of interfacial magnetic anisotropy on crystal orientation may be generally true for NM/FMI bilayers.

This manifestation of a significant interfacial magnetic anisotropy likely stems from the Rashba spin-orbit coupling at the NM/FMI interface, which was recently shown to be quite large if the NM capping layer was a d-block transition metal [17]. This agrees with the fact that the Rashba SOC can only increase the strength of the anisotropy in the plane of the film [2,16], which is consistent with $\Delta(4\pi M_{\rm eff}) > 0$ in every bilayer measured in this study. Specifically, the interfacial Rashba SOC is most likely generated from the overlap between the localized Fe^{3+} d orbitals in the oxygen terminated FMI [27] and the d orbitals in the NM [17,28,29]. Consequently, the FMI surfaces of various crystal orientations will have different bond lengths and angles to the NM, leading to varying degrees of orbital overlap and distortion of the

octahedral and tetrahedral cages enclosing the Fe^{3+} ions at the interface among the (100)-, (111)-, and (110)-oriented FMIs.

While this orbital overlap can qualitatively explain the overall effect in these bilayer systems, it is challenging to predict the strength of the effect and how its magnitude is affected by the orientation of the garnets due to their complex lattice structure. To model and understand the trend of interfacial anisotropy on crystal orientation, many parameters are needed about the materials as well as the interface such as interfacial bonding symmetry, sharpness, orbital overlap, possible charge transfer, strain, termination, band structure, etc. This reported trend on interfacial magnetic anisotropy likely induced by Rashba SOC and its dependence on crystal orientation will hopefully stimulate and provide evidence for future studies.

IV. CONCLUSIONS

In conclusion, we measure changes in effective saturation magnetization, which arises from the interfacial magnetic anisotropy, in high-quality TmIG and YIG films grown on (100)-, (111)-, and (110)-oriented GGG and capped with Pt or Au. The Pt or Au overlayer induces a significant interfacial magnetic anisotropy of the FMI films determined by the angular dependent FMR. By comparing $\Delta(4\pi M_{\text{eff}})$ for all of the (Pt or Au)/(TmIG or YIG) bilayer combinations, a consistent trend is found that the (110)-oriented films exhibit the largest $\Delta(4\pi M_{\text{eff}})$ up to 3255 G, followed by the (111)-oriented films, and finally the (100)-oriented films with the smallest values of $\Delta(4\pi M_{\text{eff}})$. This study points toward the Rashba SOC as the underlying mechanism for the interfacial magnetic anisotropy at the NM/FMI interface as well as provides an additional method for tuning the magnetic anisotropy in these bilayers, which have recently proven to host exciting new phenomena that take advantage of electrically generated spin-orbit torques.

ACKNOWLEDGMENTS

This work was supported primarily by the Center for Emergent Materials, an NSF MRSEC, under Grant No. DMR-2011876, and partially by DARPA under Grant No. D18AP00008 (sample growth) and by the US Department of Energy (DOE) under Grant No. DE-SC0001304 (magnetic characterization).

[1] C. O. Avci, A. Quindeau, C. F. Pai, M. Mann, L. Caretta, A. S. Tang, M. C. Onbasli, C. A. Ross, and G. S. D. Beach, Current-induced switching in a magnetic insulator, Nat. Mater. **16**, 309 (2017).

[2] S. Banerjee, J. Rowland, O. Erten, and M. Randeria, Enhanced Stability of Skyrmions in Two-Dimensional Chiral Magnets with Rashba Spin-Orbit Coupling, Phys. Rev. X **4**, 031045 (2014).

[3] Q. M. Shao, C. Tang, G. Q. Yu, A. Navabi, H. Wu, C. L. He, J. X. Li, P. Upadhyaya, P. Zhang, S. A. Razavi, Q. L. He, Y. W. Liu, P. Yang, S. K. Kim, C. Zheng, Y. Z. Liu, L. Pan, R. K. Lake, X. F. Han, Y. Tserkovnyak *et al.*, Role of dimensional crossover on spin-orbit torque efficiency in magnetic insulator thin films, Nat. Commun. **9**, 3612 (2018).

[4] H. X. Yang, M. Chshiev, B. Dieny, J. H. Lee, A. Manchon, and K. H. Shin, First-principles investigation of the very large perpendicular magnetic anisotropy at Fe|MgO and Co|MgO interfaces, Phys. Rev. B **84**, 054401 (2011).

[5] S. Z. Peng, M. X. Wang, H. X. Yang, L. Zeng, J. Nan, J. Q. Zhou, Y. G. Zhang, A. Hallal, M. Chshiev, K. L. Wang, Q. F. Zhang, and W. S. Zhao, Origin of interfacial perpendicular magnetic anisotropy in MgO/CoFe/metallic capping layer structures, Sci. Rep. **5**, 18173 (2015).

[6] O. Boulle, J. Vogel, H. X. Yang, S. Pizzini, D. de Souza Chaves, A. Locatelli, T. O. Menteş, A. Sala, L. D. Buda-Prejbeanu, O. Klein, M. Belmeguenai, Y. Roussigné, A. Stashkevich, S. M. Chérif, L. Aballe, M. Foerster, M. Chshiev, S. Auffret, I. M. Miron, and G. Gaudin, Room-temperature chiral magnetic skyrmions in ultrathin magnetic nanostructures, Nat. Nanotechnol. **11**, 449 (2016).

[7] C. Moreau-Luchaire, C. Moutafis, N. Reyren, J. Sampaio, C. A. F. Vaz, N. Van Horne, K. Bouzehouane, K. Garcia, C. Deranlot, P. Warnicke, P. Wohlhuter, J. M. George, M. Weigand, J. Raabe, V. Cros, and A. Fert, Additive interfacial chiral interaction in multilayers for stabilization of small individual skyrmions at room temperature, Nat. Nanotechnol. **11**, 444 (2016).

[8] S. H. Woo, K. Litzius, B. Krüger, M.-Y. Im, L. Caretta, K. Richter, M. Mann, A. Krone, R. M. Reeve, M. Weigand, P. Agrawal, I. Lemesh, M.-A. Mawass, P. Fischer, M. Kläui, and G. S. D. Beach, Observation of room-temperature magnetic skyrmions and their current-driven dynamics in ultrathin metallic ferromagnets, Nat. Mater. **15**, 501 (2016).

[9] A. Soumyanarayanan, M. Raju, A. L. Gonzalez Oyarce, A. K. C. Tan, M.-Y. Im, A. P. Petrović, P. Ho, K. H. Khoo, M. Tran, C. K. Gan, F. Ernult, and C. Panagopoulos, Tunable room-temperature magnetic skyrmions in Ir/Fe/Co/Pt multilayers, Nat. Mater. **16**, 898 (2017).

[10] Q. M. Shao, Y. W. Liu, G. Q. Yu, S. K. Kim, X. Y. Che, C. Tang, Q. L. He, Y. Tserkovnyak, J. Shi, and K. L. Wang, Topological Hall effect at above room temperature in heterostructures composed of a magnetic insulator and a heavy metal, Nat. Electron. **2**, 182 (2019).

[11] A. S. Ahmed, A. J. Lee, N. Bagués, B. A. McCullian, A. M. A. Thabt, A. Perrine, J. R. Rowland, M. Randeria, P. C. Hammel, D. W. McComb, and F. Y. Yang, Spin-Hall topological Hall effect in highly tunable pt/ferrimagnetic-insulator bilayers, Nano Lett. **19**, 5683 (2019).

[12] A. J. Lee, A. S. Ahmed, J. Flores, S. D. Guo, B. B. Wang, N. Bagués, D. W. McComb, and F. Y. Yang, Probing the Source of the Interfacial Dzyaloshinskii-Moriya Interaction Responsible for the Topological Hall Effect in Metal/$Tm_3Fe_5O_{12}$ Systems, Phys. Rev. Lett. **124**, 107201 (2020).

[13] S. Y. Xia, S. Zhang, Z. Z. Luan, L. F. Zhou, J. H. Liang, G. Liu, B. Yang, H. X. Yang, R. H. Liu, and D. Wu, Interfacial

Dzyaloshinskii-Moriya interaction between ferromagnetic insulator and heavy metal, Appl. Phys. Lett. **116**, 052404 (2020).

[14] C. O. Avci, E. Rosenberg, M. Baumgartner, L. Beran, A. Quindeau, P. Gambardella, C. A. Ross, and G. S. D. Beach, Fast switching and signature of efficient domain wall motion driven by spin-orbit torques in a perpendicular anisotropy magnetic insulator/Pt bilayer, Appl. Phys. Lett. **111**, 072406 (2017).

[15] C. O. Avci, E. Rosenberg, L. Caretta, F. Büttner, M. Mann, C. Marcus, D. Bono, C. A. Ross, and G. S. D. Beach, Interface-driven chiral magnetism and current-driven domain walls in insulating magnetic garnets, Nat. Nanotechnol. **14**, 561 (2019).

[16] C. Tang, Q. Song, C.-Z. Chang, Y. D. Xu, Y. Ohnuma, M. Matsuo, Y. W. Liu, W. Yuan, Y. Y. Yao, J. S. Moodera, S. Maekawa, W. Han, and J. Shi, Dirac surface state–modulated spin dynamics in a ferrimagnetic insulator at room temperature, Sci. Adv. **4**, eaas8660 (2018).

[17] A. J. Lee, A. S. Ahmed, B. A. McCullian, S. D. Guo, M. L. Zhu, S. S. Yu, P. M. Woodward, J. Hwang, P. C. Hammel, and F. Y. Yang, Interfacial Rashba-Effect-Induced Anisotropy in Nonmagnetic-Material–Ferrimagnetic-Insulator Bilayers, Phys. Rev. Lett. **124**, 257202 (2020).

[18] H. L. Wang, C. H. Du, Y. Pu, R. Adur, P. C. Hammel, and F. Y. Yang, Large spin pumping from epitaxial $Y_3Fe_5O_{12}$ thin films to Pt and W layers, Phys. Rev. B **88**, 100406(R) (2013).

[19] F. Y. Yang and P. C. Hammel, Topical review: FMR-driven spin pumping in $Y_3Fe_5O_{12}$-based structures, J. Phys. D: Appl. Phys. **51**, 253001 (2018).

[20] H. L. Wang, C. H. Du, Y. Pu, R. Adur, P. C. Hammel, and F. Y. Yang, Scaling of Spin Hall Angle in 3d, 4d, and 5d Metals from $Y_3Fe_5O_{12}$/Metal Spin Pumping, Phys. Rev. Lett. **112**, 197201 (2014).

[21] J. T. Brangham, K. Y. Meng, A. S. Yang, J. C. Gallagher, B. D. Esser, S. P. White, S. S. Yu, D. W. McComb, P. C. Hammel, and F. Y. Yang, Thickness dependence of spin Hall angle of Au grown on $Y_3Fe_5O_{12}$ epitaxial films, Phys. Rev. B **94**, 054418 (2016).

[22] E. Turgut, M. J. Stolt, S. Jin, and G. D. Fuchs, Topological spin dynamics in cubic FeGe near room temperature, J. Appl. Phys. **122**, 183902 (2017).

[23] C. N. Wu, C. C. Tseng, K. Y. Lin, C. K. Cheng, S. L. Yeh, Y. T. Fanchiang, M. Hong, and J. Kwo, High-quality single-crystal thulium iron garnet films with perpendicular magnetic anisotropy by off-axis sputtering, AIP Adv. **8**, 055904 (2017).

[24] A. J. Lee, J. T. Brangham, Y. Cheng, S. P. White, W. T. Ruane, B. D. Esser, D. W. McComb, P. C. Hammel, and F. Y. Yang, Metallic ferromagnetic films with magnetic damping under 1.4×10^{-3}, Nat. Commun. **8**, 234 (2017).

[25] H. L. Wang, C. H. Du, P. C. Hammel, and F. Y. Yang, Strain-tunable magnetocrystalline anisotropy in epitaxial $Y_3Fe_5O_{12}$ thin films, Phys. Rev. B **89**, 134404 (2014).

[26] C. H. Du, R. Adur, H. L. Wang, A. J. Hauser, F. Y. Yang, and P. C. Hammel, Control of Magnetocrystalline Anisotropy by Epitaxial Strain in Double Perovskite Sr_2FeMoO_6 Films, Phys. Rev. Lett. **110**, 147204 (2013).

[27] X. T. Jia, K. Liu, K. Xia, and G. E. W. Bauer, Spin transfer torque on magnetic insulators, Europhys. Lett. **96**, 17005 (2011).

[28] K. V. Shanavas, Z. S. Popović, and S. Satpathy, Theoretical model for Rashba spin-orbit interaction in *d* electrons, Phys. Rev. B **90**, 165108 (2014).

[29] K. V. Shanavas and S. Satpathy, Electric Field Tuning of the Rashba Effect in the Polar Perovskite Structures, Phys. Rev. Lett. **112**, 086802 (2014).